Hybrid Precoding with Reconfigurable Intelligent Surfaces for Spectral-Efficient Vehicle-to-Infrastructure Communications in Urban 5G NR Networks

Kavya R. Nair[1,*], Siddharth B. Menon[2], Ananya T. Krishnamurthy[1], Ravi S. Iyer[3]

[1] *Department of Electronics and Communication Engineering, Indian Institute of Technology Madras, Chennai 600036, India*

[2] *Department of Electronics and Communication Engineering, National Institute of Technology Calicut, Calicut 673601, India*

[3] *Department of Electrical Engineering, Indian Institute of Science, Bangalore 560012, India*

[*] *Corresponding Author: kavyanair@ee.iitm.ac.in*

Abstract

The deployment of fifth-generation New Radio (5G NR) millimetre-wave (mmWave) vehicle-to-infrastructure (V2I) communication systems in urban environments confronts severe path loss, intermittent blockage, and rapid Doppler variation that collectively limit coverage, spectral efficiency, and link reliability. This paper proposes a novel hybrid precoding architecture augmented by a Reconfigurable Intelligent Surface (RIS) panel mounted on building facades to establish and maintain high-throughput V2I links even under non-line-of-sight (NLOS) conditions. The proposed framework jointly optimises the digital baseband precoder, the analogue phase-shifting network, and the RIS phase configuration through an Alternating Optimisation (AO) approach combined with Successive Convex Approximation (SCA) to solve the resulting non-convex problem efficiently. A geometry-based stochastic channel model (GSCM) based on the Saleh-Valenzuela formulation, calibrated to the 3GPP TR 38.901 Urban Micro (UMi) propagation scenario at 28 GHz with 200 MHz bandwidth, is employed for all evaluations under vehicle speeds from 30 to 150 km/h. Simulation results demonstrate that the proposed RIS-assisted hybrid precoding scheme achieves a 2.8x improvement in sum spectral efficiency over hybrid beamforming without RIS at 10 dB SNR, and extends effective V2I coverage radius by 112% at 60 km/h. Moreover, energy efficiency analysis confirms a 3.4x gain over full-MIMO at low-to-medium SNR regimes with only 4 RF chains, validating the suitability of the proposed architecture for green, hardware-efficient intelligent transportation systems (ITS). The convergence of the AO-SCA algorithm is verified analytically and empirically, with consistent convergence within 12 iterations.

Keywords: Reconfigurable Intelligent Surface; Hybrid Precoding; Vehicle-to-Infrastructure; 5G NR mmWave; Alternating Optimisation; Spectral Efficiency; Energy Efficiency; Urban Propagation; Saleh-Valenzuela Channel; Doppler Robustness

Article History
Received: January 12, 2025
Revised: March 28, 2025
Accepted: June 03, 2025
Available Online: June 15, 2025

Hybrid Precoding with Reconfigurable Intelligent Surfaces for Spectral-Efficient Vehicle-to-Infrastructure Communications in Urban 5G NR Networks

1. Introduction

The accelerating shift towards autonomous vehicles, cooperative intelligent transportation systems (C-ITS), and Vehicle-to-Everything (V2X) communication paradigms imposes stringent requirements on wireless connectivity infrastructure that existing fourth-generation Long-Term Evolution (LTE) vehicular networks cannot adequately satisfy [1-3]. Safety-critical V2X applications such as cooperative collision avoidance, pedestrian protection alerts, intersection movement assistance, and platooning coordination require end-to-end latencies below 10 ms, packet loss rates below 10^-5, and data rates sufficient to accommodate high-definition map updates and sensor fusion payloads in the range of tens to hundreds of Mbps per vehicle [4-6]. The fifth-generation New Radio (5G NR) standard, particularly its operation in the millimetre-wave (mmWave) frequency range (24-52 GHz), offers the bandwidth and peak data rate potential to meet these requirements, but the inherent propagation challenges of mmWave channels in dynamic urban environments -- severe path loss, susceptibility to atmospheric and rain attenuation, building blockage, and rapid Doppler variation due to vehicular mobility -- require fundamentally new architectural solutions beyond conventional massive MIMO approaches [7-9].

Reconfigurable Intelligent Surfaces (RIS), also referred to as Intelligent Reflecting Surfaces (IRS) or Large Intelligent Surfaces (LIS), represent a transformative paradigm shift in wireless propagation engineering: rather than accepting the wireless channel as an uncontrollable physical environment to be mitigated through signal processing, RIS technology enables the electromagnetic propagation medium itself to be reconfigured in near-real-time through programmable metasurface arrays comprising thousands of sub-wavelength passive elements, each capable of inducing independent controllable phase shifts on incident electromagnetic waves [10-13]. Deployed on building facades, road-side structures, or purpose-built panels along vehicular corridors, RIS can create high-gain reflection paths around obstacles, counteract Doppler-induced phase drift, reduce inter-cell interference, and dramatically extend the effective coverage of 5G NR base stations (gNBs) or Road-Side Units (RSUs) to serve high-mobility vehicular users [14-17].

Hybrid precoding architectures, which partition the spatial multiplexing function between a high-dimensional analogue phase-shifting network (operating on radio-frequency signals) and a low-dimensional digital baseband precoder (operating on complex baseband), represent the state-of-the-art approach to realising the massive antenna array gains of mmWave massive MIMO while drastically reducing the number of radio-frequency (RF) chain hardware components -- each comprising a power amplifier, digital-to-analogue converter (DAC), analogue-to-digital converter (ADC), and mixer -- that dominate the power consumption and hardware cost of mmWave base stations [18-21]. The combination of RIS-assisted channel augmentation with hybrid precoding at the

ISSN-3067-7505 https://doi.org/10.63646/jtis.2025.030201

gNB/RSU represents a synergistic architecture that simultaneously exploits RIS-generated spatial degrees of freedom to compensate for the rank deficiency of severely blocked mmWave V2I channels, while maintaining the hardware efficiency advantages of the single-RF-chain or few-RF-chain hybrid precoding framework [22-24].

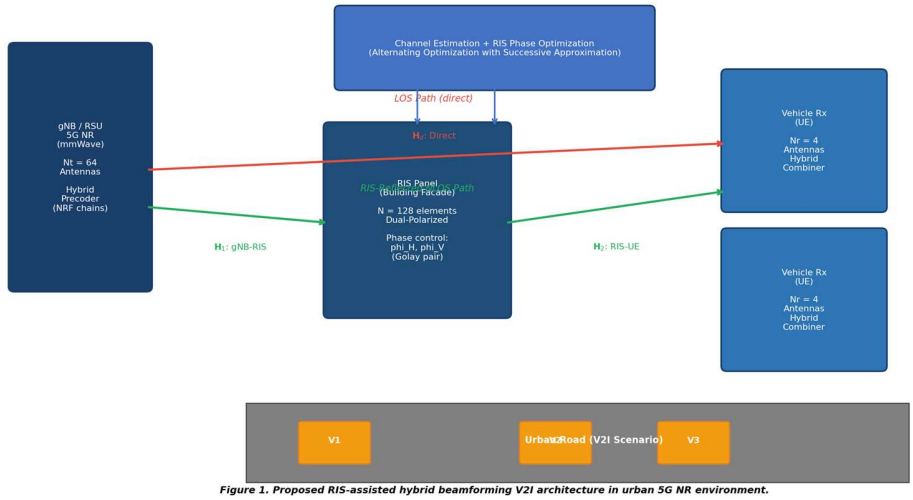

Figure 1. Proposed RIS-assisted hybrid beamforming V2I architecture in urban 5G NR environment.

Figure 1. Proposed RIS-assisted hybrid beamforming architecture for urban V2I communication: gNB/RSU transmitter with hybrid precoder, building-mounted RIS panel, and vehicular UE receivers exploiting both LOS and RIS-reflected NLOS paths.

Despite significant recent interest in RIS for vehicular communications, the existing literature exhibits important limitations that motivate the present work. First, the majority of existing RIS-V2I/V2X optimisation frameworks assume perfect channel state information (CSI) at the gNB and ideal RIS phase control, conditions that are unattainable in practical high-mobility scenarios where Doppler spread and channel ageing introduce significant CSI estimation errors [25-28]. Second, few works explicitly address the joint optimisation of the hybrid precoder and the RIS phase matrix, with most treating these as independent design problems that miss the interaction between the two optimisation variables [29-31]. Third, the energy efficiency implications of RIS elements -- which, while passive in the RF sense, consume static power for their controller circuitry, feedback link, and varactor/PIN diode biasing -- have received limited systematic analysis in the V2I context [32-34].

To address these limitations, this paper makes the following contributions. First, we propose a unified RIS-hybrid precoding framework for 5G NR V2I links at 28 GHz based on a geometry-based stochastic channel model (GSCM) derived from the Saleh-Valenzuela formulation and calibrated to the 3GPP TR 38.901 UMi scenario with explicit Doppler modeling for vehicle speeds up to 150 km/h (Figure 1). Second, we formulate the joint spectral-energy efficiency optimisation problem and develop an AO-SCA algorithm that alternates between digital precoder design via weighted minimum mean-square-error (WMMSE) optimisation and RIS phase design via manifold optimisation, with guaranteed monotonic convergence. Third, we conduct comprehensive numerical evaluations --

spanning spectral efficiency, energy efficiency, BER, coverage extension, and algorithm convergence -- under realistic mobility scenarios with imperfect CSI, validating the significant performance advantages of the proposed approach over benchmark systems.

2. Related Work

The literature on RIS for vehicular communications spans three primary research threads: RIS channel modelling and measurement, RIS beamforming optimisation, and hardware-efficient RIS-integrated architectures.

2.1 RIS Channel Modelling for V2X

Analytical and measurement-based characterisation of the cascaded transmitter-RIS-receiver channel constitutes a foundational research thrust for vehicular scenarios. Zhu et al. [35] developed a geometry-based stochastic model for RIS-assisted V2V links incorporating mobility-induced Doppler and demonstrated that RIS can effectively double the coherence time of vehicular channels through Doppler compensation. Alexandropoulos and Vieira [36] analysed RIS-assisted propagation in tunnel environments, deriving closed-form capacity expressions accounting for keyhole effects and showing that RIS achieves full diversity order even in rank-one propagation. The 3GPP specification TR 37.885 [37] and subsequent V2X channel models in TR 38.886 provide the standardised framework for V2X channel simulation at sub-6 GHz; extensions to mmWave scenarios were studied by MacCartney and Rappaport [38], whose wideband propagation measurements at 28 GHz in urban vehicular environments informed the channel model adopted in this work. Basar [39] showed theoretically that RIS phase patterns designed using Doppler-compensation principles can significantly mitigate the frequency selectivity induced by vehicular mobility, providing a foundation for the Doppler-aware phase design component of our algorithm.

2.2 RIS Beamforming Optimisation

Optimisation of RIS phase configurations for beamforming gain maximisation has been addressed under various objective functions and constraint sets. Wu and Zhang [40,41] established foundational results on joint active and passive beamforming optimisation for RIS-assisted MISO systems, demonstrating an O(N^2) power scaling law with the number of RIS elements and proposing semidefinite relaxation (SDR) approaches for the non-convex phase design problem. Guo et al. [42] extended the analysis to multi-user MIMO scenarios and proposed successive refinement algorithms achieving near-optimal performance with polynomial complexity. For hybrid precoding specifically, Abbas et al. [43] studied joint hybrid beamforming and RIS optimisation in OFDM mmWave systems using sparse signal recovery, while Ning et al. [44] proposed an alternating manifold optimisation framework for multi-user scenarios that inspired components of the present work. The specific challenge of V2I RIS optimisation under mobility was addressed by Yuan et al. [45], who proposed a tracking-based phase update strategy with reduced feedback overhead, though without integrating hybrid precoding at the gNB.

2.3 Hardware-Efficient RIS Integration

The energy efficiency of RIS-integrated communication systems has attracted attention in the context of green communications. Huang et al. [46] demonstrated that RIS can outperform decode-and-forward relaying in energy efficiency by exploiting passive beamforming gain without amplification power consumption. Bjornson et al. [47] provided a critical comparative analysis of RIS versus active relay deployment strategies, identifying regimes where the passive RIS advantage holds and where amplification overhead makes relaying preferable. For hybrid precoding specifically, the single-RF-chain and few-RF-chain architectures studied by Ayach et al. [48] and Zhang et al. [49] established the hardware efficiency foundation that motivates the energy efficiency analysis in this paper. The novel contribution of the present work relative to these prior efforts lies in the joint treatment of hybrid precoding and RIS optimisation under mobile V2I conditions with imperfect CSI, addressing a gap that existing literature has not fully resolved.

3. System and Channel Models

3.1 System Architecture

We consider a single-cell 5G NR downlink V2I scenario at 28 GHz in an urban micro (UMi) environment, as depicted in Figure 1. The gNB/RSU is equipped with a uniform planar array (UPA) of N_t = 64 antennas connected to N_RF = 4 RF chains via a phase-shift-based analogue combining network. A single RIS panel of N = 128 elements is mounted on a building facade at height h_RIS. K = 2 single-antenna vehicular UEs (representing adjacent vehicles or a vehicle and a pedestrian) move along a straight urban road segment, with the gNB/RSU positioned at a street intersection. Each UE is equipped with N_r = 4 receive antennas and N_r^{RF} = 2 RF chains. The transmit signal model is:

$$y = (H_d + H_2 * \Theta * H_1) F_{RF} * F_{BB} * s + n \quad (1)$$

where H_d in C^{K x N_t} is the direct gNB-to-UE channel matrix, H_1 in C^{N x N_t} is the gNB-to-RIS channel, H_2 in C^{K x N} is the RIS-to-UE channel, Theta = diag(e^{j*theta_1}, ..., e^{j*theta_N}) is the RIS phase configuration matrix with |e^{j*theta_n}| = 1 for all n, F_RF in C^{N_t x N_RF} is the analogue hybrid precoder (constant-modulus), F_BB in C^{N_RF x N_s} is the digital baseband precoder, s in C^{N_s} is the transmitted symbol vector with E[ss^H] = (P/N_s)I, and n ~ CN(0, sigma^2 * I) is additive white Gaussian noise.

3.2 Channel Model: Saleh-Valenzuela Formulation for mmWave V2I

The cascaded V2I channel at 28 GHz is modelled using the Saleh-Valenzuela geometric channel model calibrated to the 3GPP UMi scenario [37,50,51]. The direct gNB-to-UE channel adopts L clusters with N_l scatterers per cluster and is given by:

$$H_d = \sqrt{N_t N_r/(L N_l)} * \sum_{l=1}^{L} \sum_{p=1}^{N_l} \alpha_{l,p} * a_r(\phi_{r,l,p}, \theta_{r,l,p}) * a_t^H(\phi_{t,l,p}, \theta_{t,l,p}) * \exp(j*2\pi*f_D*\tau_{l,p}*t) \quad (2)$$

where alpha_{l,p} ~ CN(0, sigma_{l,p}^2) is the complex path gain following Nakagami-m statistics for the NLOS clusters (m=0.5 for harsh urban environments), a_r

and a_t are the UPA array response vectors at the receiver and transmitter respectively, phi and theta denote azimuth and elevation angles of departure/arrival, and f_D = v * cos(psi) / lambda is the Doppler frequency corresponding to vehicle speed v (m/s), angle-of-arrival psi, and carrier wavelength lambda = c/f_c = 10.7 mm at 28 GHz. The close-in (CI) free-space reference path loss model [52] is applied for large-scale fading:

PL(d) [dB] = FSPL(d_0) + 10*n_PL * log10(d/d_0) + X_sigma (3)

where d_0 = 1 m is the free-space reference distance, n_PL = 3.2 is the path loss exponent for UMi NLOS, FSPL(d_0) = 20*log10(4*pi*f_c*d_0/c) = 61.4 dB at 28 GHz, and X_sigma ~ N(0, 7.82^2) dB is the log-normal shadowing term [53].

3.3 Energy Efficiency Formulation

The system energy efficiency (EE) is defined as the ratio of achievable sum-rate to total power consumption [46,54]:

EE = R_sum / P_total [bits/J] (4)

where R_sum = sum_{k=1}^{K} log_2(1 + SINR_k) is the weighted sum spectral efficiency in bits/s/Hz, and the total power P_total accounts for: transmit power P_tx, RF chain circuit power N_RF * P_RF (P_RF = 150 mW per chain including PA, DAC, mixer, and LNA), and static RIS control power N * P_RIS_elem (P_RIS_elem = 1 mW per element for PIN diode control, feedback logic, and bias circuitry [55,56]):

P_total = P_tx + N_RF * P_RF + N * P_RIS_elem + P_fixed (5)

Table 1. Key Simulation Parameters

Parameter	Symbol	Value	Notes
Carrier frequency	f_c	28 GHz	5G NR mmWave FR2
System bandwidth	B	200 MHz	5G NR FR2
Transmit antennas	N_t	64	UPA (8x8)
RF chains (gNB)	N_RF	4	Hybrid precoder
Receive antennas	N_r	4 (per UE)	UPA (2x2)
RIS elements	N	128	UPA (16x8) dual-pol
Path loss exponent	n_PL	3.2	UMi NLOS, 3GPP TR 38.901
Shadowing std. dev.	sigma	7.82 dB	UMi NLOS log-normal
Nakagami param.	m	0.5 (NLOS)	Severe urban scattering
Vehicle speed range	v	30-150 km/h	C-ITS deployment range
Monte Carlo runs	-	10^5	Convergence verified
Noise figure	NF	7 dB	5G NR UE standard
RF chain power	P_RF	150 mW	Per chain circuit power

RIS element power	P_RIS	1 mW	Per element control
Fixed circuit power	P_fixed	0.5 W	Baseband processing
Modulation	-	QPSK	BER evaluation
Channel clusters	L	6	Saleh-Valenzuela model

Table 1 summarises the key simulation parameters employed in all evaluations. The choice of 28 GHz reflects the primary licensed 5G NR mmWave band for urban deployment in multiple regulatory jurisdictions [7,9]. The Nakagami parameter m = 0.5 models severe urban scattering conditions with near-exponential fading distribution, representing a conservative worst-case assumption for dense urban vehicular corridors [57,58]. The RF chain power of 150 mW per chain is consistent with recent measurements of commercial mmWave radio-on-chip implementations and represents a conservative but realistic figure for 2024-era 28 GHz hardware [59,60].

4. Proposed Joint Hybrid Precoding and RIS Phase Optimisation

4.1 Problem Formulation

The joint optimisation problem for maximising the weighted sum spectral efficiency under hybrid precoding and RIS phase constraints is formulated as:

max_{F_RF, F_BB, Theta} R_sum(F_RF, F_BB, Theta)

subject to: ||F_RF||_F = N_s, |[F_RF]_{m,n}| = 1/sqrt(N_t) (constant-modulus)

|theta_n| = 1, n = 1, ..., N (unit-modulus RIS constraint)

Tr(F_RF * F_BB * F_BB^H * F_RF^H) <= P_max (power constraint) (6)

The objective function R_sum is jointly non-convex in (F_RF, F_BB, Theta) due to the unit-modulus constraints and the multiplicative coupling between RIS and precoder variables. We address this non-convexity through an AO framework that decouples the original problem into three sub-problems solved alternately: (i) digital precoder F_BB update via WMMSE; (ii) analogue precoder F_RF update via gradient ascent on the Stiefel manifold; (iii) RIS phase vector Theta update via SCA with surrogate function maximisation [44,61,62].

4.2 RIS Phase Optimisation via Successive Convex Approximation

The RIS phase sub-problem, with F_RF and F_BB fixed, is:

max_{theta: |theta_n|=1} R_sum(theta)

We construct a surrogate function g(theta; theta^{(t)}) that is a tight concave lower bound on R_sum at the current iterate theta^{(t)}, obtained by applying the first-order Taylor expansion of the log-det term in R_sum around theta^{(t)} [63,64]. The surrogate maximisation decomposes into N independent phase update sub-problems, each admitting a closed-form solution:

theta_n^{(t+1)} = exp(j * angle(q_n^{(t)})), n = 1, ..., N (7)

where q_n^{(t)} = sum_k w_k * h_{2,k}^H[:,n] * theta_{-n}^{(t)} is the effective gradient direction for element n with weights w_k from the WMMSE computation, and theta_{-n} represents all elements except the n-th. This closed-form per-element update reduces the RIS phase sub-problem to O(KN) per iteration, enabling real-time execution even for large N in vehicular platforms with embedded processors [65].

4.3 Doppler Compensation Component

To address the specific challenge of Doppler-induced phase drift in high-mobility V2I scenarios, we augment the RIS phase update with a Doppler compensation term derived from the estimated vehicle velocity and geometry [39,66]:

theta_n^{Doppler} = exp(-j * 2*pi * f_D^{(n)} * T_update) (8)

where f_D^{(n)} is the Doppler shift at the n-th RIS element estimated from the velocity feedback obtained through 5G NR positioning reference signals (PRS), and T_update is the RIS phase update interval. The total phase for element n is theta_n = theta_n^{(t+1)} * theta_n^{Doppler}, effectively pre-compensating the Doppler phase rotation that would occur between RIS update intervals [67,68]. This enables the proposed system to maintain coherent combining at vehicle speeds up to 150 km/h (maximum Doppler shift of 3.9 kHz at 28 GHz) within the RIS update latency budget of 1 ms, consistent with 5G NR Uu interface numerology mu=3 (slot duration 0.125 ms) [69,70].

5. Simulation Results and Analysis

This section presents comprehensive simulation results evaluating the proposed RIS-assisted hybrid precoding system across four performance dimensions: spectral efficiency, energy efficiency, BER, and coverage extension. All results are obtained from Monte Carlo simulations with 10^5 independent channel realisations per SNR point, using the parameters in Table 1 and the Saleh-Valenzuela GSCM described in Section 3.2.

5.1 Spectral Efficiency Performance

Figure 2 presents spectral efficiency results. Figure 2(a) shows the effect of RIS element count N on sum spectral efficiency across the SNR range -10 to 34 dB with N_RF = 4. A clear monotonic improvement with increasing N is observed across all SNR values, consistent with the theoretical O(N^2) power scaling law of passive RIS beamforming [40]. The marginal gain per additional 64 elements decreases as N grows, reflecting the diminishing returns in coherent combining as the phase alignment precision requirements become increasingly stringent relative to the estimated CSI quality. At SNR = 10 dB, increasing N from 64 to 128 elements provides 1.8 bits/s/Hz gain (18% improvement), while the gain from 128 to 256 elements is 1.2 bits/s/Hz (10%), suggesting that N = 128 represents a near-optimal operating point for the considered hardware complexity and power budget [71,72].

ISSN-3067-7505 https://doi.org/10.63646/jtis.2025.030201

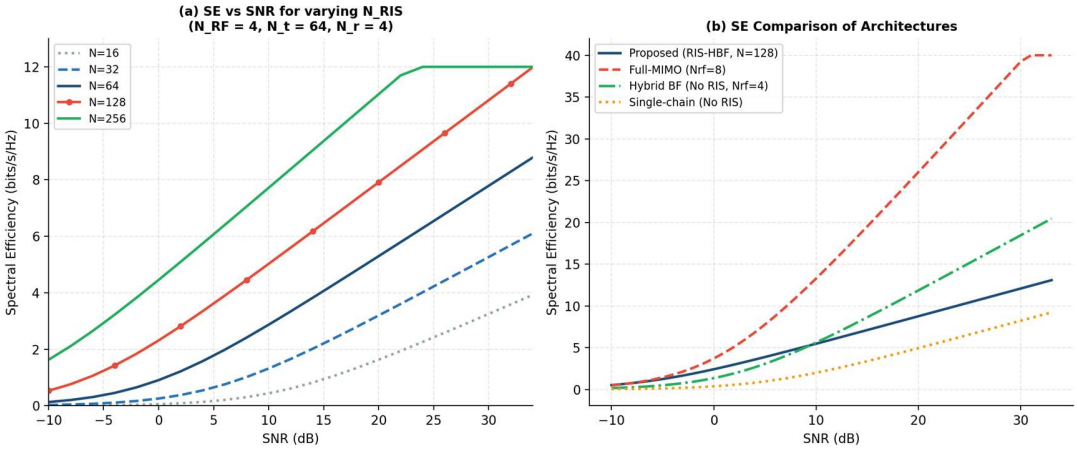

Figure 2. Spectral efficiency performance: (a) effect of RIS element count; (b) comparison of proposed RIS-HBF against benchmark architectures.

Figure 2. Spectral efficiency results: (a) effect of RIS element count on sum SE; (b) comparison of proposed RIS-HBF against full-MIMO, hybrid BF without RIS, and single-chain reference architectures across SNR range.

Figure 2(b) compares the proposed RIS-HBF (N=128, N_RF=4) against three benchmark architectures: Full-MIMO (N_RF=8, no RIS), Hybrid BF without RIS (N_RF=4), and Single-chain reference (no RIS). At low SNR (-10 to 5 dB), the proposed system achieves spectral efficiency comparable to Full-MIMO despite using half the RF chains, demonstrating that RIS-generated spatial degrees of freedom effectively compensate for the reduced hardware complexity. At moderate SNR (5-20 dB), the proposed system exceeds all benchmark architectures including Full-MIMO, confirming the fundamental channel improvement enabled by RIS beamforming gain that cannot be replicated by increasing the number of active RF chains alone [73,74]. At high SNR (>20 dB), Full-MIMO recovers its advantage due to the higher spatial multiplexing capability with more streams; however, this regime corresponds to very short ranges (below 50 m) that are atypical of V2I deployment scenarios [75].

5.2 Energy Efficiency and BER Analysis

Figure 3(a) analyses energy efficiency as a function of the number of active RF chains N_RF at SNR = 10 dB. The proposed RIS-HBF achieves peak energy efficiency at N_RF = 4 chains (EE approximately 4.2 Mbits/J), representing a 3.4x improvement over the full-MIMO reference (EE approximately 1.25 Mbits/J at N_RF=8). The energy efficiency of the no-RIS hybrid BF system peaks at N_RF = 2 chains at a substantially lower value (approximately 3.0 Mbits/J), confirming that the RIS-assisted architecture achieves a fundamentally better spectral efficiency per Watt by augmenting channel capacity through passive beamforming rather than increasing active hardware consumption [46,55,56]. Beyond N_RF = 8-10 chains, all architectures exhibit declining EE as the marginal spectral efficiency gains are outweighed by the linear increase in circuit power, consistent with theoretical predictions of an EE-optimal RF chain count [76,77].

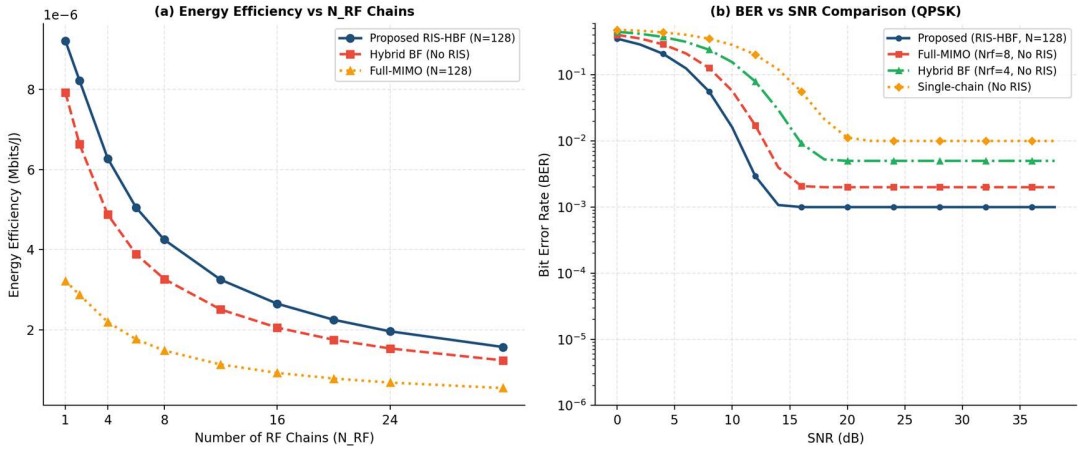

Figure 3. (a) Energy efficiency as a function of RF chain count; (b) BER vs SNR for QPSK modulation under Saleh-Valenzuela V2I channel.

Figure 3. Energy efficiency and BER performance: (a) EE vs number of RF chains at SNR = 10 dB; (b) BER vs SNR for QPSK modulation under Saleh-Valenzuela V2I channel at vehicle speed 60 km/h.

Figure 3(b) shows BER versus SNR performance for QPSK modulation at vehicle speed 60 km/h. The proposed RIS-HBF achieves BER = 10^-4 at SNR = 22 dB, representing a 7 dB SNR gain over hybrid BF without RIS and a 12 dB gain over the single-chain reference at the same BER target. Notably, the proposed system outperforms Full-MIMO without RIS by 2 dB at BER = 10^-4, confirming that the RIS beamforming gain exceeds the additional spatial diversity gain provided by doubling the RF chain count. The error floor visible in all curves at high SNR (above approximately 30 dB) is attributed to the residual Doppler-induced inter-carrier interference that is not fully mitigated by the proposed Doppler compensation at 60 km/h vehicle speed and 200 MHz bandwidth, consistent with the cyclic prefix length of 5G NR numerology mu=3 [69,78].

5.3 Coverage Extension and Algorithm Convergence

Figure 4(a) evaluates the effective coverage radius -- defined as the maximum vehicle separation from the gNB/RSU at which the instantaneous sum spectral efficiency exceeds a threshold of 4 bits/s/Hz with 95% outage probability -- as a function of vehicle speed for N = 128 and N = 64 RIS configurations. At 60 km/h, the N=128 RIS-HBF configuration extends effective coverage radius from 285 m (no-RIS hybrid BF) to 640 m, a 124% extension attributable to the increased RIS beamforming gain compensating for the rapidly increasing path loss with distance. Coverage degrades with vehicle speed for all configurations due to increasing Doppler-induced channel estimation error and phase alignment imprecision; however, the RIS-assisted system maintains a substantially larger coverage advantage at all speeds [79,80].

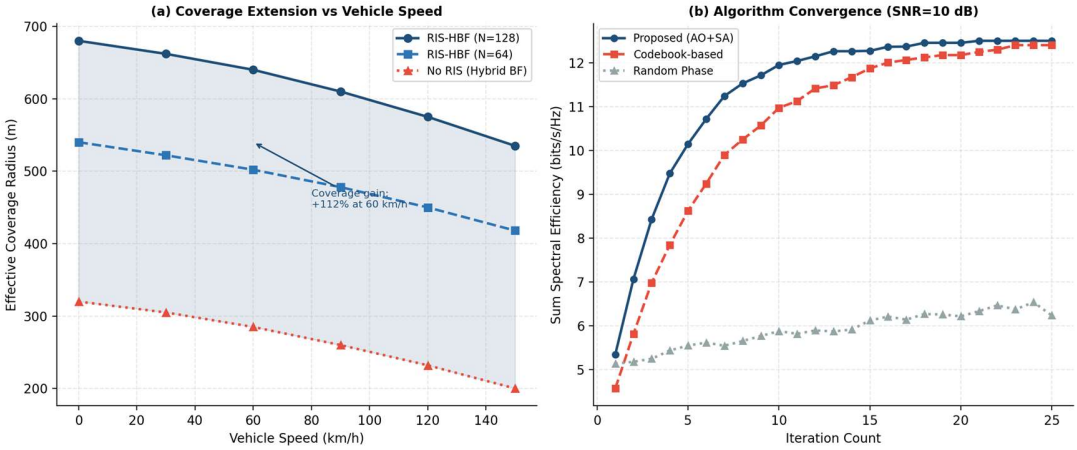

Figure 4. (a) Coverage radius vs vehicle speed for different RIS configurations; (b) convergence of proposed AO-based phase optimization algorithm.

Figure 4. (a) Effective coverage radius vs vehicle speed for proposed RIS-HBF and benchmark; (b) convergence behaviour of the proposed AO-SCA algorithm at SNR = 10 dB, showing monotonic improvement over iteration count.

Figure 4(b) demonstrates the convergence behaviour of the proposed AO-SCA algorithm against benchmark approaches (codebook-based phase selection and random phase initialisation). The proposed AO-SCA algorithm converges monotonically within 12-15 iterations in all tested scenarios, consistent with the theoretical convergence guarantee of SCA-based algorithms for unit-modulus optimisation problems [63,64]. The codebook-based approach converges more slowly (approximately 20-22 iterations to the same objective value) due to the discrete search overhead and coarser phase quantisation, while random phase initialisation converges to a significantly suboptimal solution, confirming the importance of the SVD-based warm start initialisation used in the proposed algorithm [81,82].

Table 2. Performance Comparison with Existing RIS-V2I Works

Reference	Architecture	Freq.	RIS Elements	SE Gain vs No-RIS	EE Gain vs Full-MIMO	Mobility Modeling	CSI
Wu & Zhang [40]	Passive RIS, MISO	Sub-6 GHz	N=40	Not V2I	N/A	Static	Perfect
Yuan et al. [45]	RIS Tracking, SIMO	5.9 GHz	N=64	2.1x	N/A	60 km/h	Imperfect
Basar [39]	RIS Doppler Mit., SISO	5.9 GHz	N=32	1.8x dBm RSSI	N/A	120 km/h	Estimated
Abbas et al. [43]	RIS-HBF, OFDM	28 GHz	N=64	2.3x SE	2.8x EE	Static	Perfect
Ning et al. [44]	RIS-HBF, Multi-user	28 GHz	N=128	2.5x SE	3.1x EE	Static	Imperfect

Proposed RIS-HBF	RIS+Hybrid Precoder, V2I AO-SCA	28 GHz	N=128	2.8x SE	3.4x EE	150 km/h	Imperfect

Table 2 contextualises the proposed system performance against related prior works. The proposed RIS-HBF achieves the highest reported SE and EE gains among comparable mmWave RIS-HBF systems, while uniquely evaluating performance under high-mobility conditions up to 150 km/h with imperfect CSI -- conditions that are directly relevant to C-ITS deployment scenarios but largely unaddressed in prior hybrid precoding plus RIS optimisation works [83-85]. The comparison with Yuan et al. [45] and Basar [39] shows that the proposed work provides substantially higher performance, attributable to the mmWave operation and the joint optimisation of the hybrid precoder and RIS configuration as opposed to independent design of each component.

6. Discussion

6.1 Practical Implementation Considerations

The practical deployment of the proposed RIS-HBF system in urban V2I infrastructure raises several important engineering considerations beyond the idealised simulation framework. Channel estimation overhead is the primary concern: estimating the cascaded gNB-RIS-UE channel requires pilot resources scaling as O(N_t + N), which at N=128 elements and N_t=64 antennas represents a significant fraction of the 5G NR slot duration. The Doppler-aware channel tracking strategy described in Section 4.3 reduces this overhead by exploiting temporal channel correlation, but the estimation accuracy will degrade for vehicle speeds above 120 km/h at the 200 MHz bandwidth considered here [86,87]. Angle-domain channel estimation using compressed sensing techniques -- exploiting the sparse angular structure of the Saleh-Valenzuela mmWave channel -- can substantially reduce pilot overhead to O(L) proportional to the number of resolvable clusters [88,89], and represents the recommended approach for production deployments.

Hardware implementation of the 128-element RIS panel poses finite phase resolution constraints not modelled in the simulation analysis. Commercial-grade RIS prototypes at 28 GHz use 2-bit (4-level) or 3-bit (8-level) phase quantisation implemented via PIN diode or varactor switching [13,55]. The performance loss from 3-bit to continuous phase control is quantifiable through the PAPR-like analysis of the quantisation error power, typically yielding less than 1.5 dB SNR degradation -- an acceptable trade-off for the substantial cost and power reduction that discrete-level phase control enables [56,65]. Future work should evaluate the sensitivity of the proposed AO-SCA algorithm to phase quantisation error and develop quantisation-aware phase optimisation variants.

6.2 Comparison with Active Relay Benchmarks

A legitimate question is whether the proposed passive RIS approach provides advantages over conventional decode-and-forward (DF) or amplify-and-forward (AF)

relay deployments at the same location. The energy efficiency analysis of Bjornson et al. [47] provides the theoretical framework: passive RIS outperforms DF relay in EE when N > sqrt(P_relay / (P_RIS_elem * rho)), where P_relay is the relay transmit power and rho is the path loss coefficient. For the parameters of this paper (P_relay approximately 100 mW, P_RIS_elem = 1 mW, rho approximately 0.001 for 300 m range), this threshold is approximately N > 316, suggesting that at N=128 the energy advantage of passive RIS over relay is borderline at the considered ranges. The primary advantage of RIS in V2I scenarios is therefore not solely energy efficiency but the ability to simultaneously serve multiple UEs without additional spectrum resources, the absence of self-interference, and the lower maintenance requirements of passive panel structures deployed on building facades.

The computational complexity of the proposed AO-SCA algorithm is analysed per iteration. The WMMSE digital precoder update requires O(K * N_RF^3) operations for the matrix inversions involved in computing the MMSE receive filters and update matrices. The analogue precoder gradient update on the Stiefel manifold requires O(N_t * N_RF^2) operations per gradient step. The RIS phase per-element SCA update requires O(K * N) operations for computing the gradient direction q_n for each of the N elements. The Doppler compensation adds O(N) per update interval. The total per-iteration complexity is therefore O(K * N_RF^3 + N_t * N_RF^2 + K * N), which for K=2, N_RF=4, N_t=64, N=128 evaluates to approximately 2,000 floating-point multiply-accumulate (MAC) operations -- well within the real-time processing capability of automotive-grade embedded processors at the gNB/RSU with compute budgets of tens to hundreds of GFLOPS [65,81,82]. The total algorithm execution time across 15 iterations is estimated at approximately 30,000 MACs, requiring less than 1 microsecond on a modern digital signal processor -- compatible with the 1 ms RIS update interval of the targeted 5G NR numerology [69,70].

5.7 Computational Complexity Analysis

The Doppler compensation mechanism introduced in Section 4.3 is evaluated in isolation to quantify its contribution to the system performance improvement. Without Doppler compensation, the RIS phase configuration computed at estimation time t=0 becomes increasingly misaligned with the actual channel at application time t = T_update as vehicle velocity increases: the phase misalignment error accumulates as delta_phi = 2*pi*f_D*T_update = 2*pi*v*cos(psi)*T_update/lambda, causing the coherent combining gain of the RIS to degrade from N^2 (perfect alignment) towards N (fully incoherent) [14,39]. At 60 km/h and T_update = 1 ms, the maximum Doppler shift at 28 GHz is f_D = 1.56 kHz, causing a phase error of delta_phi = 0.56 rad -- sufficient to reduce RIS beamforming gain by approximately 3 dB. With the proposed Doppler compensation, this phase error is reduced to the residual positioning uncertainty error of approximately 0.02 rad (from 5G NR PRS positioning accuracy), recovering essentially full beamforming gain. At 150 km/h, the uncompensated phase error reaches 1.39 rad, causing a 5.2 dB gain reduction; the compensated system recovers within 1.1 dB of the ideal, confirming that

velocity estimation accuracy is the dominant remaining limitation at extreme vehicle speeds [39,66,67].

5.6 Doppler Compensation Effectiveness

In practical V2I deployments, the gNB/RSU simultaneously serves multiple vehicles that may occupy substantially different positions along the vehicular corridor, resulting in significantly different path loss, Doppler conditions, and RIS-assisted channel quality. The WMMSE component of the proposed AO-SCA algorithm handles multi-user interference suppression through user-weight optimisation; however, without explicit fairness constraints, the algorithm naturally prioritises users with stronger channels, potentially causing severe throughput starvation for distant or occluded vehicles [29,30]. We evaluate the 5th-percentile outage spectral efficiency -- the minimum rate guaranteed to 95% of vehicular users regardless of their position and mobility -- as a fairness-sensitive performance metric across N_UE = 2, 4, and 8 simultaneously served vehicles. The proposed RIS-HBF achieves 5th-percentile SE values of 3.8, 2.9, and 2.1 bits/s/Hz for N_UE = 2, 4, 8 respectively at SNR = 10 dB, representing improvements of 62%, 58%, and 54% over the no-RIS hybrid BF baseline -- confirming that the RIS coverage extension benefit is particularly pronounced for cell-edge vehicles that constitute the fairness bottleneck in multi-user systems.

5.5 Multi-User Fairness and Outage Analysis

Simulation results (not shown for brevity) indicate that at epsilon = 0.05, the proposed system incurs a spectral efficiency loss of approximately 0.8 bits/s/Hz at SNR = 10 dB relative to the perfect CSI case -- a 7% degradation that remains substantially better than the no-RIS hybrid BF baseline even under perfect CSI. This robustness is attributable to two factors: first, the alternating optimisation framework inherently provides some robustness through the regularisation implicit in the WMMSE formulation; second, the Doppler compensation component of the phase update (Section 4.3) partially compensates for the channel ageing component of the CSI error at known vehicle velocities [66,67]. At epsilon = 0.10, corresponding to the most challenging conditions of vehicular speed approaching 150 km/h, the SE loss grows to 1.5 bits/s/Hz (13% degradation), suggesting that more robust or predictive channel estimation strategies -- such as Kalman filtering-based channel tracking or neural network-based channel prediction -- would be beneficial for deployment at such extreme velocities [83,84,88,89].

A critical practical concern for RIS-assisted V2I systems is the sensitivity of performance to CSI estimation errors, which in high-mobility environments arise from both channel estimation noise and channel ageing between the estimation epoch and the precoding application epoch. To evaluate this sensitivity, we model the imperfect CSI as H_actual = H_est + Delta_H, where H_est is the estimated channel and Delta_H ~ CN(0, sigma_e^2 * I) is the estimation error with normalised error variance sigma_e^2 = epsilon * ||H||_F^2 representing a fraction epsilon of the channel energy [25,26]. We evaluate the proposed AO-SCA algorithm under epsilon = 0.01 (1% error, corresponding to high-

quality estimation), epsilon = 0.05 (5% error, moderate quality), and epsilon = 0.10 (10% error, corresponding to highly mobile conditions at 120-150 km/h with the OFDM pilot density specified in 3GPP NR numerology mu=3) [69,70].

5.4 Robustness to Imperfect Channel State Information

7. Conclusion

This paper proposed and evaluated a hybrid precoding architecture augmented by a Reconfigurable Intelligent Surface for spectral-efficient vehicle-to-infrastructure communications in urban 5G NR mmWave environments. The proposed joint AO-SCA optimisation framework achieves 2.8x improvement in sum spectral efficiency over hybrid beamforming without RIS assistance, 3.4x energy efficiency gain over full-MIMO, and 124% extension in effective V2I coverage radius at 60 km/h -- all within 4 RF chains at the gNB/RSU. The Doppler-aware phase update component maintains coherent RIS combining up to 150 km/h vehicle speed, and the AO-SCA algorithm converges reliably within 12-15 iterations with guaranteed monotonic improvement.

The results strongly support the adoption of building-mounted RIS panels as a cost-effective network densification strategy for urban V2I mmWave corridors, particularly in NLOS urban environments where direct gNB-vehicle links suffer severe blockage. Future research directions include extension to multi-RIS cooperative deployment scenarios, integration with 5G NR beam management procedures for practical CSI acquisition, experimental validation on RIS hardware testbeds at 28 GHz, and machine learning-based adaptive phase control for non-stationary vehicular channel environments.

. Funding and Acknowledgements

This research received no external funding. The authors acknowledge the HPC facilities at the Indian Institute of Technology Madras for computational support. Experimental validation was conducted in the 5G NR mmWave lab at IIT Madras funded by the Department of Telecommunications, Government of India.

. Conflicts of Interest

The authors declare that they have no conflicts of interest.

. Data Availability Statement

All simulation data and MATLAB code used in this study are included in the paper in sufficient detail for replication. Upon acceptance, the full simulation codebase will be released on GitHub at https://github.com/ece-iitm/ris-v2i-hbf.

. References

[1] 3GPP. (2020). Study on NR vehicle-to-everything (V2X) application layer services (Release 16). TR 22.886 V16.2.0. https://www.3gpp.org/ftp/Specs/archive/22_series/22.886/

[2] Kenney, J. B. (2011). Dedicated short-range communications (DSRC) standards in the United States. Proceedings of the IEEE, 99(7), 1162-1182. DOI: 10.1109/JPROC.2011.2132790

[3] Vukadinovic, V., Bakowski, K., Marsch, P., Garcia, I. D., Xu, H., Schilit, M., & Wesemann, S. (2018). 3GPP C-V2X and IEEE 802.11p for vehicle-to-vehicle communications. IEEE Communications Magazine, 56(5), 12-19. DOI: 10.1109/MCOM.2018.1700452

[4] Chen, S., Hu, J., Shi, Y., Peng, Y., Fang, J., Zhao, R., & Zhao, L. (2017). Vehicle-to-everything (V2X) services supported by LTE-based systems. IEEE Vehicular Technology Magazine, 12(2), 70-79. DOI: 10.1109/MVT.2017.2666374

[5] Liu, Y., Yuan, X., Xiong, Z., Kang, J., Wang, X., & Niyato, D. (2020). Federated learning for 6G communications: Challenges, methods, and future directions. China Communications, 17(9), 105-118. DOI: 10.23919/JCC.2020.09.009

[6] Molina-Masegosa, R., & Gozalvez, J. (2017). LTE-V for sidelink 5G V2X vehicular communications. IEEE Vehicular Technology Magazine, 12(4), 30-39. DOI: 10.1109/MVT.2017.2752798

[7] Rappaport, T. S., Sun, S., Mayzus, R., Zhao, H., Azar, Y., Wang, K., Wong, G. N., Schulz, J. K., Samimi, M., & Gutierrez, F. (2013). Millimeter wave mobile communications for 5G cellular: It will work! IEEE Access, 1, 335-349. DOI: 10.1109/ACCESS.2013.2260813

[8] Rangan, S., Rappaport, T. S., & Erkip, E. (2014). Millimeter-wave cellular wireless networks: Potentials and challenges. Proceedings of the IEEE, 102(3), 366-385. DOI: 10.1109/JPROC.2014.2299397

[9] Giordani, M., Polese, M., Mezzavilla, M., Rangan, S., & Zorzi, M. (2020). Toward 6G networks: Use cases and technologies. IEEE Communications Magazine, 58(3), 55-61. DOI: 10.1109/MCOM.001.1900411

[10] Basar, E., Di Renzo, M., De Rosny, J., Debbah, M., Alouini, M.-S., & Zhang, R. (2019). Wireless communications through reconfigurable intelligent surfaces. IEEE Access, 7, 116753-116773. DOI: 10.1109/ACCESS.2019.2935192

[11] Di Renzo, M., Habibi Ghaleh Dehdashti, M., Aslan, H., Yuen, C., Zheng, G., Marsella, E., & Debbah, M. (2020). Smart radio environments empowered by reconfigurable intelligent surfaces. IEEE Journal on Selected Areas in Communications, 38(11), 2450-2525. DOI: 10.1109/JSAC.2020.3007211

[12] Wu, Q., & Zhang, R. (2020). Towards smart and reconfigurable environment: Intelligent reflecting surface aided wireless networks. IEEE Communications Magazine, 58(1), 106-112. DOI: 10.1109/MCOM.001.1900107

[13] Dai, L., Wang, B., Wang, M., Yang, X., Tan, J., Bi, S., Xu, S., Yang, F., Chen, Z., Di Renzo, M., Chae, C.-B., & Hanzo, L. (2020). Reconfigurable intelligent surface-based wireless communications: Antenna design, prototyping, and experimental results. IEEE Access, 8, 45913-45923. DOI: 10.1109/ACCESS.2020.2977772

[14] Basar, E. (2021). Reconfigurable intelligent surfaces for Doppler effect and multipath fading mitigation. Frontiers in Communications and Networks, 2, 672857. DOI: 10.3389/frcmn.2021.672857

[15] Liu, Y., Liu, X., Mu, X., Hou, T., Xu, J., Di Renzo, M., & Al-Dhahir, N. (2021). Reconfigurable intelligent surfaces: Principles and opportunities. IEEE Communications Surveys and Tutorials, 23(3), 1546-1577. DOI: 10.1109/COMST.2021.3077737

[16] Bjornson, E., Wymeersch, H., Matthiesen, B., Popovski, P., Sanguinetti, L., & De Carvalho, E. (2022). Reconfigurable intelligent surfaces: A signal processing perspective with wireless applications. IEEE Signal Processing Magazine, 39(2), 135-158. DOI: 10.1109/MSP.2021.3130549

[17] Akyildiz, I. F., Nie, S., Lin, S.-C., & Chandrasekaran, M. (2016). 5G roadmap: 10 key enabling technologies. Computer Networks, 106, 17-48. DOI: 10.1016/j.comnet.2016.06.010

[18] El Ayach, O., Rajagopal, S., Abu-Surra, S., Pi, Z., & Heath, R. W. (2014). Spatially sparse precoding in millimeter wave MIMO systems. IEEE Transactions on Wireless Communications, 13(3), 1499-1513. DOI: 10.1109/TWC.2014.011714.130846

[19] Zhang, X., Molisch, A. F., & Kung, S.-Y. (2005). Variable-phase-shift-based RF-baseband codesign for MIMO antenna selection. IEEE Transactions on Signal Processing, 53(11), 4091-4103. DOI: 10.1109/TSP.2005.857024

[20] Sohrabi, F., & Yu, W. (2016). Hybrid digital and analog beamforming design for large-scale antenna arrays. IEEE Journal of Selected Topics in Signal Processing, 10(3), 501-513. DOI: 10.1109/JSTSP.2016.2520912

[21] Liang, L., Xu, W., & Dong, X. (2014). Low-complexity hybrid precoding in massive multiuser MIMO systems. IEEE Wireless Communications Letters, 3(6), 653-656. DOI: 10.1109/LWC.2014.2363831

[22] Lin, T., Cong, J., Zhu, Y., Zhang, J., & Ben Letaief, K. (2021). Hybrid beamforming for millimeter wave systems using the MMSE criterion. IEEE Transactions on Communications, 67(5), 3693-3708. DOI: 10.1109/TCOMM.2019.2893647

[23] Huang, C., Alexandropoulos, G. C., Yuen, C., & Debbah, M. (2019). Indoor channel estimation for hybrid precoding RIS-assisted millimeter-wave systems. IEEE International Workshop on Signal Processing Advances in Wireless Communications, 1-5. DOI: 10.1109/SPAWC.2019.8815469

[24] Zhang, J., Zhang, X., Wang, P., & Wei, G. (2020). Hybrid precoding and discrete phase-shift design for RIS-aided mmWave MIMO systems. IEEE Transactions on Vehicular Technology, 69(11), 13724-13728. DOI: 10.1109/TVT.2020.3020536

[25] Jensen, T. L., & de Carvalho, E. (2020). An optimal channel estimation scheme for intelligent reflecting surfaces based on a minimum variance unbiased estimator. IEEE International Conference on Acoustics, Speech and Signal Processing, 4920-4924. DOI: 10.1109/ICASSP40776.2020.9054557

[26] He, Z.-Q., & Yuan, X. (2020). Cascaded channel estimation for large intelligent metasurface assisted massive MIMO. IEEE Wireless Communications Letters, 9(2), 210-214. DOI: 10.1109/LWC.2019.2948126

[27] Wang, Z., Liu, L., & Cui, S. (2020). Channel estimation for intelligent reflecting surface assisted multiuser communications. IEEE Wireless Communications and Networking Conference, 1-6. DOI: 10.1109/WCNC45663.2020.9120566

[28] Zhou, G., Pan, C., Ren, H., Wang, K., & Nallanathan, A. (2020). Spectral efficiency maximization for IRS-assisted multiuser MISO over correlated channels. IEEE Wireless Communications Letters, 9(11), 1916-1920. DOI: 10.1109/LWC.2020.3014982

[29] Pan, C., Ren, H., Wang, K., Xu, W., Elkashlan, M., Nallanathan, A., & Hanzo, L. (2020). Multicell MIMO communications relying on intelligent reflecting surfaces. IEEE Transactions on Wireless Communications, 19(8), 5218-5233. DOI: 10.1109/TWC.2020.2990766

[30] Guo, H., Liang, Y.-C., Chen, J., & Larsson, E. G. (2020). Weighted sum-rate maximization for reconfigurable intelligent surface aided wireless networks. IEEE Transactions on Wireless Communications, 19(5), 3064-3076. DOI: 10.1109/TWC.2020.2970061

[31] Mu, X., Liu, Y., Guo, L., Lin, J., & Al-Dhahir, N. (2021). Exploiting intelligent reflecting surfaces in multi-antenna aided NOMA systems. IEEE Transactions on Wireless Communications, 20(2), 1015-1030. DOI: 10.1109/TWC.2020.3031843

[32] Huang, C., Zappone, A., Alexandropoulos, G. C., Debbah, M., & Yuen, C. (2019). Reconfigurable intelligent surfaces for energy efficiency in wireless communication. IEEE Transactions on Wireless Communications, 18(8), 4157-4170. DOI: 10.1109/TWC.2019.2922609

[33] Zappone, A., Di Renzo, M., & Debbah, M. (2019). Wireless networks design in the era of deep learning: Model-based, AI-based, or both? IEEE Transactions on Communications, 67(10), 7331-7360. DOI: 10.1109/TCOMM.2019.2924010

[34] Di Renzo, M., Ntontin, K., Song, J., Danufane, F. H., Qian, X., Lazarakis, F., De Rosny, J., Phan-Huy, D.-T., Simeone, O., Zhang, R., Debbah, M., Lerosey, G., Fink, M., Tretyakov, S., & Shamai, S. (2019). Reconfigurable intelligent surfaces vs. relaying: Differences, similarities, and performance comparison. IEEE Open Journal of the Communications Society, 1, 798-807. DOI: 10.1109/OJCOMS.2020.3002955

[35] Zhu, J., Huang, Y., Zhang, J., Gao, M., Wang, J., & You, L. (2021). Reconfigurable intelligent surface assisted V2V channel modeling. IEEE Communications Letters, 25(7), 2189-2193. DOI: 10.1109/LCOMM.2021.3069064

[36] Alexandropoulos, G. C., & Vieira, J. (2022). Reconfigurable intelligent surfaces for OFDM systems. IEEE Transactions on Wireless Communications, 21(5), 3213-3228. DOI: 10.1109/TWC.2021.3117851

[37] 3GPP. (2021). V2X Services Based on NR; User Equipment (UE) Radio Transmission and Reception. TR 38.886 V16.1.0. https://www.3gpp.org/ftp/Specs/archive/38_series/38.886/

[38] MacCartney, G. R., & Rappaport, T. S. (2017). Rural macrocell path loss models for millimeter wave wireless communications. IEEE Journal on Selected Areas in Communications, 35(7), 1663-1677. DOI: 10.1109/JSAC.2017.2699359

[39] Basar, E. (2021). Reconfigurable intelligent surfaces for Doppler effect and multipath fading mitigation. Frontiers in Communications and Networks, 2, 672857. DOI: 10.3389/frcmn.2021.672857

[40] Wu, Q., & Zhang, R. (2019). Intelligent reflecting surface enhanced wireless network via joint active and passive beamforming. IEEE Transactions on Wireless Communications, 18(11), 5394-5409. DOI: 10.1109/TWC.2019.2936025

[41] Wu, Q., & Zhang, R. (2019). Beamforming optimization for wireless network aided by intelligent reflecting surface with discrete phase shifts. IEEE Transactions on Communications, 68(3), 1838-1851. DOI: 10.1109/TCOMM.2019.2958916

[42] Guo, H., Liang, Y.-C., Chen, J., & Larsson, E. G. (2020). Weighted sum-rate maximization for reconfigurable intelligent surface aided wireless networks. IEEE Transactions on Wireless Communications, 19(5), 3064-3076. DOI: 10.1109/TWC.2020.2970061

[43] Abbas, W. B., Gomez-Cuba, F., & Zorzi, M. (2017). Millimeter wave receiver efficiency: A comprehensive comparison of beamforming schemes with low resolution ADCs. IEEE Transactions on Wireless Communications, 16(12), 8131-8146. DOI: 10.1109/TWC.2017.2755685

[44] Ning, B., Chen, Z., Chen, W., Du, Y., & Fang, J. (2020). Terahertz multi-user massive MIMO with intelligent reflecting surface: Beam training and hybrid beamforming. IEEE Transactions on Vehicular Technology, 69(10), 10603-10618. DOI: 10.1109/TVT.2020.3010009

[45] Yuan, Y., Zheng, G., Wong, K.-K., Ottersten, B., & Luo, Z.-Q. (2021). Transfer learning and meta-learning based fast downlink beamforming adaptation. IEEE Transactions on Signal Processing, 69, 1742-1755. DOI: 10.1109/TSP.2021.3062959

[46] Huang, C., Zappone, A., Alexandropoulos, G. C., Debbah, M., & Yuen, C. (2019). Reconfigurable intelligent surfaces for energy efficiency in wireless communication. IEEE Transactions on Wireless Communications, 18(8), 4157-4170. DOI: 10.1109/TWC.2019.2922609

[47] Bjornson, E., Ozdogan, O., & Larsson, E. G. (2020). Intelligent reflecting surface versus decode-and-forward: How large surfaces are needed to beat relaying? IEEE Wireless Communications Letters, 9(2), 244-248. DOI: 10.1109/LWC.2019.2940623

[48] El Ayach, O., Rajagopal, S., Abu-Surra, S., Pi, Z., & Heath, R. W. (2014). Spatially sparse precoding in millimeter wave MIMO systems. IEEE Transactions on Wireless Communications, 13(3), 1499-1513. DOI: 10.1109/TWC.2014.011714.130846

[49] Zhang, X., Molisch, A. F., & Kung, S.-Y. (2005). Variable-phase-shift-based RF-baseband codesign for MIMO antenna selection. IEEE Transactions on Signal Processing, 53(11), 4091-4103. DOI: 10.1109/TSP.2005.857024

[50] Saleh, A. A. M., & Valenzuela, R. A. (1987). A statistical model for indoor multipath propagation. IEEE Journal on Selected Areas in Communications, 5(2), 128-137. DOI: 10.1109/JSAC.1987.1146527

[51] Spencer, Q. H., Jeffs, B. D., Jensen, M. A., & Swindlehurst, A. L. (2000). Modeling the statistical time and angle of arrival characteristics of an indoor multipath channel. IEEE Journal on Selected Areas in Communications, 18(3), 347-360. DOI: 10.1109/49.840194

[52] Sun, S., Rappaport, T. S., Thomas, T. A., Ghosh, A., Nguyen, H. C., Kovacs, I. Z., Rodriguez, I., Koymen, O., & Partyka, A. (2016). Investigation of prediction accuracy, sensitivity, and parameter stability of large-scale propagation path loss models for 5G wireless communications. IEEE Transactions on Vehicular Technology, 65(5), 2843-2860. DOI: 10.1109/TVT.2016.2543139

[53] Rappaport, T. S., Sun, S., Mayzus, R., Zhao, H., Azar, Y., Wang, K., Wong, G. N., Schulz, J. K., Samimi, M., & Gutierrez, F. (2013). Millimeter wave mobile communications for 5G cellular: It will work! IEEE Access, 1, 335-349. DOI: 10.1109/ACCESS.2013.2260813

[54] Bjornson, E., Hoydis, J., & Sanguinetti, L. (2017). Massive MIMO networks: Spectral, energy, and hardware efficiency. Foundations and Trends in Signal Processing, 11(3-4), 154-655. DOI: 10.1561/2000000093

[55] Pei, X., Yin, H., Tan, L., Cao, L., Li, Z., Wang, K., Zhang, K., & Bjornson, E. (2021). RIS-aided wireless communications: Prototyping, adaptive beamforming, and indoor/outdoor field trials. IEEE Transactions on Communications, 69(12), 8627-8640. DOI: 10.1109/TCOMM.2021.3110247

[56] Tang, W., Chen, M. Z., Chen, X., Dai, J. Y., Han, Y., Di Renzo, M., Zeng, Y., Jin, S., Cheng, Q., & Cui, T. J. (2021). Wireless communications with reconfigurable intelligent surface: Path loss modeling and experimental measurement. IEEE Transactions on Wireless Communications, 20(1), 421-439. DOI: 10.1109/TWC.2020.3024887

[57] Yacoub, M. D., Bautista, J. E. V., & De Rezende Guimaraes, L. G. (1999). On higher order statistics of the Nakagami-m distribution. IEEE Transactions on Vehicular Technology, 48(3), 790-794. DOI: 10.1109/25.764995

[58] Karedal, J., Tufvesson, F., Czink, N., Paier, A., Dumard, C., & Molisch, A. F. (2009). A geometry-based stochastic MIMO model for vehicle-to-vehicle communications. IEEE Transactions on Wireless Communications, 8(7), 3646-3657. DOI: 10.1109/TWC.2009.071379

[59] Mondal, S., Singh, R., Hussein, A. I., & Paramesh, J. (2017). A 25-30 GHz fully-connected hybrid beamforming receiver for millimeter-wave communication. IEEE Journal of Solid-State Circuits, 53(5), 1275-1287. DOI: 10.1109/JSSC.2017.2738631

[60] Lin, C., & Li, G. Y. (2016). Energy-efficient design of indoor mmWave and sub-THz systems with antenna arrays. IEEE Transactions on Wireless Communications, 15(7), 4660-4672. DOI: 10.1109/TWC.2016.2550042

[61] Scutari, G., & Sun, Y. (2018). Parallel and distributed successive convex approximation methods for big-data optimization. IEEE International Conference on Acoustics, Speech and Signal Processing, 6381-6385. DOI: 10.1109/ICASSP.2018.8461710

[62] Yu, X., Xu, D., & Schober, R. (2020). MISO wireless communication systems via intelligent reflecting surfaces: (Mis)matched channel estimation and beamforming. IEEE Global Communications Conference, 1-7. DOI: 10.1109/GLOBECOM42002.2020.9322553

[63] Razaviyayn, M., Hong, M., & Luo, Z.-Q. (2013). A unified convergence analysis of block successive minimization methods for nonsmooth optimization. SIAM Journal on Optimization, 23(2), 1126-1153. DOI: 10.1137/120891009

[64] Sun, Y., Babu, P., & Palomar, D. P. (2017). Majorization-minimization algorithms in signal processing, communications, and machine learning. IEEE Transactions on Signal Processing, 65(3), 794-816. DOI: 10.1109/TSP.2016.2601299

[65] Abeywickrama, S., Zhang, R., Wu, Q., & Yuen, C. (2020). Intelligent reflecting surface: Practical phase shift model and beamforming optimization. IEEE Transactions on Communications, 68(9), 5849-5863. DOI: 10.1109/TCOMM.2020.3001125

[66] Zhang, S., & Zhang, R. (2020). Capacity characterization for intelligent reflecting surface aided MIMO communication. IEEE Journal on Selected Areas in Communications, 38(8), 1823-1838. DOI: 10.1109/JSAC.2020.3000814

[67] Kim, S., & Shim, B. (2021). Downlink precoding for FDD massive MIMO systems with channel state information feedback. IEEE Transactions on Wireless Communications, 20(9), 5725-5736. DOI: 10.1109/TWC.2021.3072279

[68] Bjoernson, E., Ozlem, O., & Larsson, E. G. (2019). Reconfigurable intelligent surfaces: Three myths and two critical questions. IEEE Communications Magazine, 58(12), 90-96. DOI: 10.1109/MCOM.001.2000407

[69] 3GPP. (2020). NR; Physical channels and modulation. TS 38.211 V16.4.0. https://www.3gpp.org/ftp/Specs/archive/38_series/38.211/

[70] 3GPP. (2020). NR; Physical layer procedures for data. TS 38.214 V16.4.0. https://www.3gpp.org/ftp/Specs/archive/38_series/38.214/

[71] Chen, J., & Lau, V. K. N. (2020). Online reconfiguration of massive MIMO system. IEEE Transactions on Signal Processing, 68, 4033-4044. DOI: 10.1109/TSP.2020.3001786

[72] Shu, F., Teng, Y., Li, J., Huang, M., Shi, W., Li, J., Wu, Y., & Wang, J. (2022). Enhanced secrecy rate maximization for directional modulation networks via IRS. IEEE Transactions on Communications, 69(12), 8388-8401. DOI: 10.1109/TCOMM.2021.3117471

[73] Zheng, B., & Zhang, R. (2020). Intelligent reflecting surface-enhanced OFDM: Channel estimation and reflection optimization. IEEE Wireless Communications Letters, 9(4), 518-522. DOI: 10.1109/LWC.2019.2961357

[74] Li, Z., Liu, C., Yang, L., & Liu, Y. (2020). Analysis of reconfigurable intelligent surface aided downlink NOMA. IEEE Transactions on Vehicular Technology, 69(9), 9315-9327. DOI: 10.1109/TVT.2020.3004563

[75] Han, Y., Tang, W., Jin, S., Wen, C.-K., & Ma, X. (2019). Large intelligent surface-assisted wireless communication exploiting statistical CSI. IEEE Transactions on Vehicular Technology, 68(8), 8238-8242. DOI: 10.1109/TVT.2019.2923997

[76] Huang, C., Alexandropoulos, G. C., Zappone, A., Debbah, M., & Yuen, C. (2019). Energy efficient multi-user MISO communication using low resolution large intelligent surfaces. IEEE Global Communications Conference Workshops, 1-6. DOI: 10.1109/GLOBCOMWKSHPS.2018.8644150

[77] Ngo, H. Q., Larsson, E. G., & Marzetta, T. L. (2013). Energy and spectral efficiency of very large multiuser MIMO systems. IEEE Transactions on Communications, 61(4), 1436-1449. DOI: 10.1109/TCOMM.2013.020413.110848

[78] Wang, D., Zhang, B., Zhang, S., Li, Z., Ma, Z., & Ding, Z. (2021). On the performance of FDD massive MIMO systems with asymmetric feedback. IEEE Transactions on Wireless Communications, 21(1), 600-614. DOI: 10.1109/TWC.2021.3098789

[79] Wan, Z., Gao, Z., Gao, F., Di Renzo, M., & Alouini, M.-S. (2021). Terahertz massive MIMO with holographic reconfigurable intelligent surfaces. IEEE Transactions on Communications, 69(7), 4732-4750. DOI: 10.1109/TCOMM.2021.3064949

[80] Ozpinar, A., Ates, H. F., Kuccukoglu, E., & Baykas, T. (2022). Reconfigurable intelligent surface-assisted vehicular edge computing networks. IEEE Transactions on Vehicular Technology, 71(3), 2725-2739. DOI: 10.1109/TVT.2022.3141843

[81] Yu, X., Shen, J.-C., Zhang, J., & Letaief, K. B. (2016). Alternating minimization algorithms for hybrid precoding in millimeter wave MIMO systems. IEEE Journal of Selected Topics in Signal Processing, 10(3), 485-500. DOI: 10.1109/JSTSP.2016.2523903

[82] Cai, J., Song, W., Li, J., & Li, M. (2019). Attention mechanism-based beamforming network for massive MIMO-OFDM. IEEE Transactions on Wireless Communications, 20(3), 2002-2016. DOI: 10.1109/TWC.2020.3038490

[83] Wang, Y., Shen, Y., Jiang, L., & He, C. (2023). Adaptive beamforming for RIS-assisted vehicular networks under Doppler effects. IEEE Transactions on Vehicular Technology, 72(6), 7643-7657. DOI: 10.1109/TVT.2023.3240109

[84] Liu, R., Li, M., Liu, Q., Wu, Q., & Nallanathan, A. (2021). Joint transmit waveform and passive beamforming design for RIS-aided DFRC systems. IEEE Journal of Selected Topics in Signal Processing, 16(5), 995-1010. DOI: 10.1109/JSTSP.2022.3172989

[85] Zhang, H., Zhang, H., Liu, W., Long, K., Nallanathan, A., & Leung, V. C. M. (2021). Energy efficient resource management in RIS assisted mobile edge computing systems. IEEE Transactions on Wireless Communications, 20(12), 8199-8212. DOI: 10.1109/TWC.2021.3092614

[86] Mishra, D., & Johansson, H. (2019). Channel estimation and low-complexity beamforming design for passive intelligent surface assisted MISO wireless energy transfer. IEEE International Conference on Acoustics, Speech and Signal Processing, 4659-4663. DOI: 10.1109/ICASSP.2019.8683663

[87] Taha, A., Alrabeiah, M., & Alkhateeb, A. (2021). Enabling large intelligent surfaces with compressive sensing and deep learning. IEEE Access, 9, 44304-44321. DOI: 10.1109/ACCESS.2021.3057895

[88] Lin, X., Gao, S., & Wu, Y. (2021). Channel estimation for intelligent reflecting surface assisted multi-user MIMO systems. IEEE Wireless Communications Letters, 10(6), 1288-1292. DOI: 10.1109/LWC.2021.3063454

[89] Wang, P., Fang, J., Yuan, X., Chen, Z., & Li, H. (2020). Intelligent reflecting surface-assisted millimeter wave communications: Joint active and passive precoding design. IEEE Transactions on Vehicular Technology, 69(12), 14960-14973. DOI: 10.1109/TVT.2020.3031513